ISSN: 0067-2904

Micro structures, Morphology and Optical Properties of Sb_2O_3: WO_3, In_2O_3 Nanostructure Composite Thin Films

Mohammed I. Tareq, Bushra A. Hasan
Department of physics, collage of science, university of Baghdad, Baghdad, Iraq

Received: 29/3/2023 Accepted: 30/8/2023 Published: 30/10/2024

Abstract

This work is concerned with the synthesis of two types of composites thin films (Sb_2O_3:WO_3 and (Sb_2O_3:In_2O_3) with different concentrations (0.0,0.05,0.1, and 0.15). The prepared thin films are characterized with the use of the X-ray diffraction atomic force microscope AFM and UV-Vis–infrared spectrophotometer. The structural examination shows that both composite's thin films were polycrystalline with nano size with cubic phase as majority and orthorhombic phase as minority phase. The crystal size decreases from 34.6 to 24.7 and 21.7 nm for (Sb_2O_3:WO_3) and (Sb_2O_3:In_2O_3) thin films, respectively. The average roughness shows non-regular growth by increasing the concentration of both oxides. The optical energy band gap shows a red shift for both types of nanostructure thin films, which populate these composited thin films for solar cell applications.

Keywords: Antimony trioxide, tungsten oxide, indium oxide, pulsed laser deposition, thin films, nanostructure, X-ray diffraction, optical properties.

التركيب الميكروي ،المورفولوجي والخواص البصرية لمتراكبات اغشية اوكسيد الانتمون :اوكسيد التنكستن، اوكسيد الانديوم ذي التراكيب النانوية

محمد عماد طارق, بشرى عباس حسن
قسم الفيزياء, كلية العلوم, جامعة بغداد, بغداد, العراق

الخلاصة

يعنى هذا البحث بتحضير نوعين من متراكبات الاغشية الرقيقة وهي اوكسيد الانتمون:اوكسيد التنكستن واكسيد الانتمون: اوكسيد الانديوم بتراكيزمختلفة **(0.0,0.05,0.1,and 0.15)**.تم تشخيص الاغشية المحضرة باستخدام حيود الاشعة السينية,مطياف القوى الذريةوالمطياف البصري عند المنطقة فوق البفسجية والمرئية وتحت الحمراء. اظهر الفحص التركيبي لكلا النوعين من متراكبات الاغشية الرقيقة كانت متعددة البلورات وبتركيب نانووي وبطور مكعب كطور رئيس وطور معيني قائم كطور ثانوي. لقد وجد ان الحجم البلوري قد تناقص من**34.6** الى**24.7**والى**21.7** نانوميترلاغشية **(Sb_2O_3:WO_3)** واغشية**(Sb_2O_3:In_2O_3)**وعلى التوالي .اظهر معدل الخشونة زيادة غير منتظمة مع زيادة تركيز كلا الاوكسيدين .اظهرت فجوة الطاقة البصرية انحراف نحو المنطقة تحت الحمراء القريبة لكلا نوعي الاغشية الرقيقة النانوية والتي تؤهل هذه متراكبات هذه الاغشية في تطبيقات الخلايا الشمسية.

*Email: mohammed.imad.tareq@gmail.com

1-Introduction

Several works [1] have examined various methods for producing and characterizing V–VI group compounds thin films. These semiconductors include antimony trioxide (Sb_2O_3). As a result of its optical, structural, photoelectronic, and electrical characteristics [2], it is a material of such relevance in the fields of both technical applications and fundamental research. For the development and design of thin-film devices, such as low loss, high reflecting mirrors utilized for various high-power laser and interferometric applications in the UV and visible spectrum [3], data on the optical constants, which include the absorption coefficient(α), refractive index(n) and optical band gap(Eg) of the thin semiconductor films are required [4]. These material's thin films have numerous desirable optical properties, such as high transmittance at visible and infrared wavelengths and high absorption in the ultraviolet region [5]. The electrical and structural characteristics of several V-VI semiconducting compounds, such as (Sb_2S_3) and(Sb_2O_3) thin films, were indicated in several earlier works [1,6]. The cubic phase, senarmontite, and the orthorhombic phase, valentinite, are crystalline forms of (Sb_2O_3) [7,8]. Similar to other semiconductor oxides, orthorhombic nano- and microstructures of nanostructured Sb_2O_3 were reported for use in nanotechnology. Solution routes were used to develop orthorhombic-elongated low-dimensional structures. Because of their innovative or exceptional qualities relative to bulk materials. Nano-materials have gained significant attention during the last ten years as material forms for technological applications and scientific research. Much research has been done on the structures, synthesis, and characteristics of semiconductor NP materials. The research of semiconducting metal oxide nanoparticles is an area of great interest [9]. Despite the comparatively limited studies on (Sb_2O_3) nanostructures compared to other semiconducting oxides that have been more thoroughly studied, such as SnO_2, ZnO, or TiO_2, there are several results on self-assembly mechanisms in (Sb_2O_3).

In the present study, thin films containing various concentrations of (Sb_2O_3:WO_3, In_2O_3) nanocrystals were produced. XRD and UV-Vis-NIR studies were used to analyze the generated (Sb_2O_3:WO_3, In_2O_3) nanocrystals thin films (Sb_2O_3) with smaller particle sizes that were created by pulsed laser deposition (PLD).

2-Experimental

In this work, Sb_2O_3, WO_3, and In_2O_3 oxides with high purity (99.999) were supplied from Aldrich company. Different composites with various concentrations according to atomic weight were prepared. The two types of composite (Sb_2O_3:WO_3 and Sb_2O_3:In_2O_3) were put in a quartz ampoule with a length of approximately 25cm and an internal diameter ~ 8mm, evacuated to about 10^{-3} Torr, heated in an oven at 913K, left at this temperature for one hour and then left to cool at the room temperature. The ampoule was then broken, and the material was extracted manually, grinded and pressed into pellets of 1 cm in diameter and 0.5 cm in thickness. Two types of composite samples from pure Sb_2O_3: (Sb_2O_3:WO_3) and (Sb_2O_3:In_2O_3), with a variety of mixing ratios (0.05, 0.1, and 0.15) were prepared by the pulsed laser deposition method. The deposition was performed in a vacuum of $2x10^{-2}$ Torr using Nd: YAG laser beam (with a pulse of 300 shoots, energy of 300mJ, and frequency of 6Hz), which was focused through a window onto the target. Ablated atoms were deposited on glass substrates to form thin films.

The film thickness (t) can be expressed by:

$$t = \frac{\lambda}{2}\frac{\Delta x}{x} \quad [10] \qquad (1)$$

Where: Δx, x, and λ represent shifting between interference fringes, the distance between interference fringes and wavelength of He:Ne laser (632.3 nm), respectively.

Crystal structure and crystallinity of (Sb_2O_3:WO_3) and (Sb_2O_3:In_2O_3) thin films were determined using XRD with the CuKα radiation (λ= 1.5406Å). The optical measurements were made using a UV-visible spectrophotometer 180 (Shimadzu UV-1800. Made in Japan); the scanning range (190-1100) nm was used to determine both the absorbance and the transmittance of the (Sb_2O_3:WO_3, In_2O_3) thin films. Crystal size (C.S), dislocation density(δ), and strain (***ε***) of the prepared thin films were conducted when FWHM or β is known using the following relations:

$$C.S = \frac{0.9\lambda}{\beta\cos\theta} \qquad \text{(Scherrer equation) [11]} \tag{2}$$

Where θ is Bragg angle.

$$\delta = \frac{1}{(C.S)^2} \tag{3}$$

and

$$\varepsilon = \frac{C.S.\cos\delta}{4} \tag{4}$$

The absorption coefficient α was calculated from equation (5):

$$\alpha = 2.303A/t \tag{5}$$

Where: A denoted the absorbance and t thickness of the film.

Optical band gap energy was estimated using Tauc relation for directly permitted transitions:

$$(\alpha h\nu) = B(h\nu - E_g)^r \text{ [12]} \tag{6}$$

Where: B is a constant, hν is the photon energy, and E_g is the optical band gap energy.

Equations utilized to calculate optical constants, the extinction coefficient(k), refractive index(n), real ε_r, and imaginary ε_i dielectric constants, are:

$$n = \left(\frac{4R}{(R-1)^2} - k^2\right)^{\frac{1}{2}} - \frac{(R+1)}{(R-1)} \tag{7}$$

$$R = \frac{(n-1)^2 + k^2}{(n+1)^2 + k^2} \tag{8}$$

$$\varepsilon_r = n^2 - k^2 \tag{9}$$

$$\varepsilon_i = 2nk \tag{10}$$

Where: n is the refractive index, R is the reflectance, K is the extinction coefficient, ε_r is the real dielectric constant, and ε_i is the imaginary dielectric constant [13]

In that order, transmittance (T) and absorption (A) tests were carried out, and the reflectance was estimated using the equation:

$$R = 1 - (A + T) \text{ [12]} \tag{11}$$

3- Results and discussion

3-1 Structural properties

3-1-1 Structural properties of Sb_2O_3:WO_3 thin films

X-ray diffraction pattern of Sb_2O_3:WO_3 nanostructures thin film composites of different WO_3 concentrations, presented in Figure 1, proved the poly-crystalline structure of these prepared thin films. The impact of an increase in the mixing ratio on crystallinity is well noticed. It can be observed from this figure that the labelled strong peaks of diffraction at 2θ= 27.71º, 46.26º, 32.14°, 35.16°, and 54.91°corresponds to diffraction planes (222), (440), (400), (420), and (622), respectively can be indexed to cubic structure according to the standard card number 96-900-7610. This result agrees with that of Qi et al. [9].

There is also a peak located at 28.39º corresponding to the plane (121) which is indexed to orthorhombic structure. The intensity of the secondary peak is observed to vanish with an

increase in WO_3 concentration [14]. The transformation from orthorhombic to cubic is ascribed to the laser irradiation.

No diffraction peaks related to metallic antimony(Sb) was noticed. XRD pattern shows peaks of hexagonal tungsten at high WO_3 concentration observed at 2θ=22.6 and 26.8º corresponding to the planes (001) and (101), respectively. This result agrees with that of Shakoury et al. [15].

The broad reflection peaks of X-ray diffraction suggest nanostructures of the prepared thin films. The crystal size of Sb_2O_3:WO_3 thin films was determined by applying the Debye–Scherrer equation (Eq. 2) considering the FWHM of the (222), (121), and (002) peaks. The average size of the Sb_2O_3:WO_3 thin films nanocrystallites was estimated and listed in Table 1. These peaks' intensity changed with increasing the WO_3 concentration in Sb_2O_3:WO_3. The 2ndphase of the antimony oxide plays a significant role in micro-structure development [7]. The diffraction peaks intensity of (222) and (121) decreased, and their FWHM increased with increasing WO3 concentration in Sb_2O_3:WO_3. These changes in the crystallinity could result from the changes in the atomic environment due to foreign WO_3 mixing with the Sb_2O_3 thin film samples.

Reduction in crystalline structure was noticed, which suggested that most W atoms have been incorporated in the Sb_2O_3 lattice. This result is attributed to a slight lattice mismatch between the radii of Sb^{3+}(0.076nm) and W^{6+} (0.065nm), and it has indicated that W ions systematically substituted Sb ions without deteriorating their crystal structure. The crystallite size estimated from the Debye–Scherrer formula was reduced from 34 to 24nm with increasing WO_3 content in the Sb_2O_3:WO_3. Crystallite size decrease was correlated with the large developed surface of the grain boundaries, thereby, resulting in larger scattering effects. Another reason for the crystallite size decrease might be a result of the drag force that is exerted by the mixing ions on the boundary motions and grain growth. WO_3 concentration increase results in the progressive reduction of antimony concentration in the system; because of this, diffusivity decreases in Sb_2O_3, and leading to suppressed grain growth of the Sb_2O_3:WO_3 samples. Simultaneously, substituted W ions provide retarding force on grain boundaries. In the case when the generated retarding force is more than the driving force for grain growth due to Sb, the movement of the grain boundary is impeded [16], which in turn results in the gradual decrease in the crystallize size with the increase in the concentration of WO_3. The strain and the dislocation density were evaluated and listed in Table 1. It is clear that strain increases from 0.001 to 0.0014 by increasing the WO_3 concentration from 0 to 0.15. The dislocation density changes with the WO_3 concentration follow the same behavior.

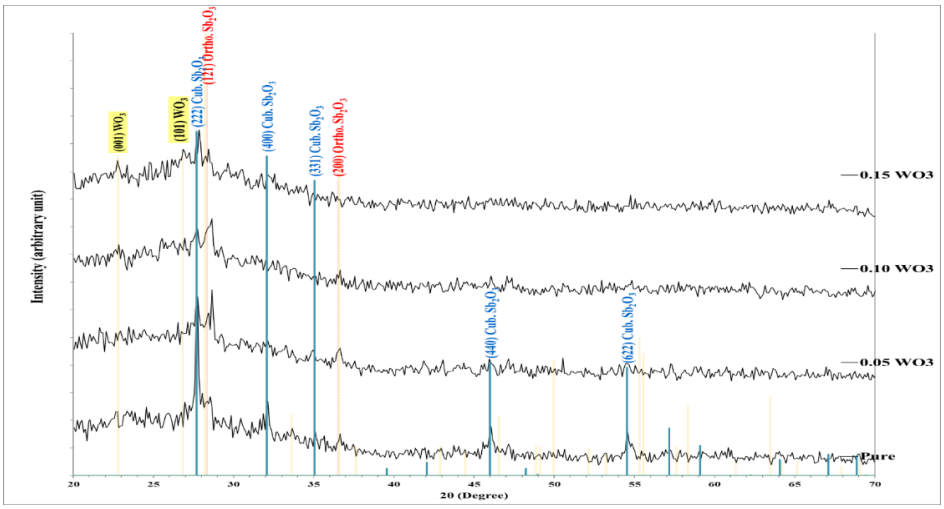

Figure 1: XRD patterns for Sb_2O_3:WO_3 nanostructures composite thin films of different WO_3 concentrations.

Table 1: XRD data for Sb_2O_3:WO_3 nanostructures composites thin films of different WO_3 concentrations.

Sample	2θ (Degrees)	FWHM (Deg.)	d_{hkl} Exp.(Å)	C.S. (nm)	hkl	Phase	δx10^{15} (line/m^2)	ε
Pure Sb_2O_3	27.7541	0.2364	3.2117	34.6	(222)	Cub. Sb_2O_3	0.83	0.0010
	28.3924	0.4728	3.1410	17.3	(121)	Ortho. Sb_2O_3	3.33	0.0020
	32.1513	0.3309	2.7818	25.0	(400)	Cub. Sb_2O_3	1.60	0.0014
	35.0591	0.3310	2.5575	25.2	(331)	Cub. Sb_2O_3	1.58	0.0014
	46.0520	0.4728	1.9693	18.3	(231)	Ortho. Sb_2O_3	3.00	0.0019
	54.5863	0.5201	1.6799	17.2	(113)	Ortho. Sb_2O_3	3.38	0.0020
0.05	27.7541	0.3073	3.2117	26.6	(222)	Cub. Sb_2O_3	1.41	0.0013
	28.4161	0.4255	3.1384	19.3	(121)	Ortho. Sb_2O_3	2.70	0.0018
	32.1040	0.4728	2.7858	17.5	(400)	Cub. Sb_2O_3	3.27	0.0020
	34.9409	0.4019	2.5658	20.7	(331)	Cub. Sb_2O_3	2.33	0.0017
	36.5721	0.4728	2.4551	17.7	(200)	Ortho. Sb_2O_3	3.19	0.0020
	45.9811	0.4492	1.9722	19.2	(231)	Ortho. Sb_2O_3	2.71	0.0018
	54.5154	0.4728	1.6819	18.9	(113)	Ortho. Sb_2O_3	2.80	0.0018
0.1	22.8132	0.4728	3.8949	17.1	(001)	Hex.WO_3	3.40	0.0020
	27.6832	0.4019	3.2198	20.4	(222)	Cub. Sb_2O_3	2.41	0.0017
	28.6288	0.4965	3.1156	16.5	(121)	Ortho. Sb_2O_3	3.67	0.0021
0.15	22.7187	0.3309	3.9109	24.5	(001)	Hex.WO_3	1.67	0.0014
	26.8794	0.4964	3.3142	16.5	(101)	Hex.WO_3	3.69	0.0021
	27.8487	0.3310	3.2010	24.7	(222)	Cub. Sb_2O_3	1.64	0.0014
	28.2742	0.4964	3.1538	16.5	(121)	Ortho. Sb_2O_3	3.67	0.0021
	32.1513	0.5201	2.7818	15.9	(400)	Cub. Sb_2O_3	3.96	0.0022

3-1-2 Structural properties of Sb_2O_3:In_2O_3 thin films

Structural identification and variation in the crystalline nature of the Sb_2O_3:In_2O_3 thin films with a change in In_2O_3 concentration are examined using the X-ray diffraction method. Figure 2 presents XRD patterns of Sb_2O_3:In_2O_3 thin films with different In_2O_3 concentrations. It is obvious that all of the prepared thin films proved to be of poly-crystalline structure and present typical diffraction pattern of cubic antimony oxide, as well as orthorhombic phase with strong peaks of diffraction at 2θ= 27.71º, 46.26º, 32.14°, 35.16°, and 54.91°corresponding to diffraction planes (222), (440), (400), (420), and (622), respectively in addition to 2θ of 28.39º corresponding to the plane (121) which can be indexed to cubic and orthorhombic structure according to the standard card No. 96-900-7610, 96-900-8063. No diffraction peaks related to indium oxide can be noticed at all. Such a result suggests that atoms of indium oxide are well-diffused in prepared thin films with no disconnections of the indium oxide phase. The FWHM for the intense (222) peak was estimated for crystalline films. The FWHM variation of the (222) peak with the In_2O_3 concentration is presented in Table 2. The value of the FWHM for the (222) peak of Sb_2O_3 thin film was measured to be 0.2364, increasing to 0.3783 by increasing the indium oxide concentration to 0.15, indicating

its nanostructure behavior which consequently reduced the crystal size of the prepared thin films. This behavior can be explained depending on many factors, such as i-the separation of indium atoms along the boundary of inter-particle at a high mixing ratio, ii-high mixing ratio establishing newer centers of growth, (iii) reorientation effects of the crystal becoming predominant at high mixing ratio [17]. All these factors contribute to the nanostructure of the prepared thin films.

The crystallite size (D) corresponding to the most intense peak was estimated from the peak position (hkl) and the FWHM [11], as shown in Table 2. The values of C.S decreased from 34.6 to 21.7 nm by increasing the indium oxide concentration from 0 to 0.15. This reduction of crystallite size may be attributed to the collection of indium atoms along the region of grain boundary, leading to the production of hindering force. When this force becomes higher than grain growth's driving force, grain boundary movement is curbed, reducing average crystallite size [18]. The location of the (222) peak has shown non-regular shifting towards lower 2θ angles with the increase of the indium oxide concentration. Such non-regular variation in the 2θ values could be due to the longer ionic radius of the incorporated In $^{3+}$(~0.8Å) compared to that of the Sb^{3+}host ions (~0.65Å). Based on Vegard's law [19,20], incorporating impurity ions of longer ionic radii in shorter ionic radii lattice results in lattice expansion as a result of the substitutional incorporations, resulting in the shifting of the diffraction peaks towards lower 2θ angles. Inter-planar distance of the (222) plane (d_{222}) was also calculated using of Bragg's equation, $2d\sin\theta = \bar{n}\lambda$, as listed in Table 2.

It is clear that the value of d_{222} increases by increasing the indium oxide concentration. The location variations of the predominate peak towards lower 2θ angles and the noticeable increase in (d_{222}) value indicate that antimony oxide expansion is a result of indium. Such host lattice expansion would yield stress in prepared thin films, which could arise due to various factors such as distortions and defects and also deviation of ionic size of the host; the added ions produce intrinsic stress in deposited films. Table 2 shows the lattice strain values of Sb_2O_3:In_2O_3 thin films. It is observed that the strain value increases from 0.001 to 0.0016 by increasing the indium oxide concentration from 0 to 0.15. The density of the dislocation(δ), which represents the length of dislocation lines per unit volume, also showed the same behavior.

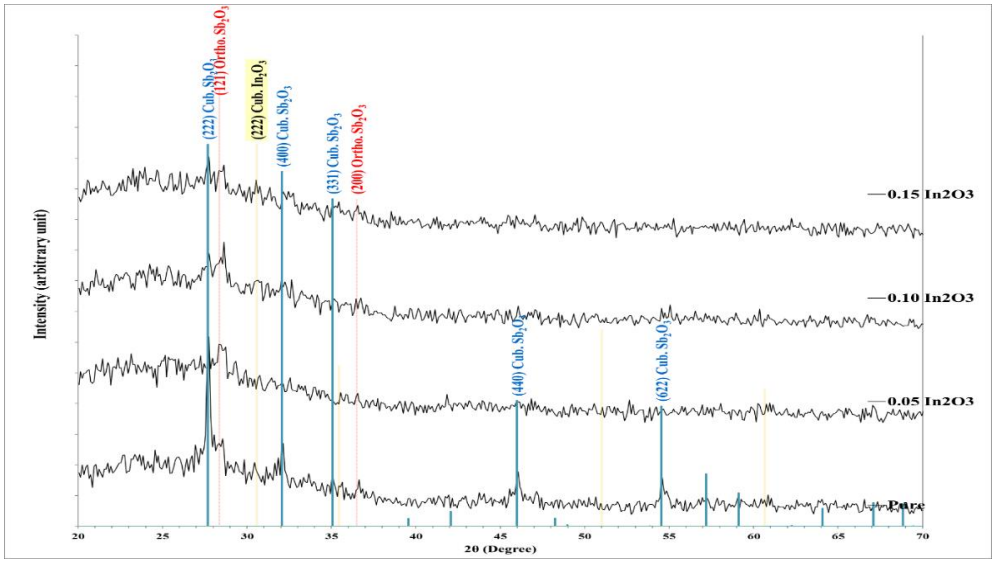

Figure 2: XRD patterns for Sb_2O_3:In_2O_3 nanostructures composites thin films of different In_2O_3 concentrations

Table 3: The XRD data for Sb_2O_3:In_2O_3 nanostructures composites thin films of different In_2O_3 concentrations

Sample	2θ (Degree)	FWHM (Deg.)	d_{hkl} Exp.(Å)	C.S. (nm)	hkl	Phase	$\delta x10^{15}$ (line/m^2)	ε
Pure Sb_2O_3	27.7541	0.2364	3.2117	34.6	(222)	Cub. Sb_2O_3	0.83	0.0010
	28.3924	0.4728	3.1410	17.3	(121)	Ortho. Sb_2O_3	3.33	0.0020
	32.1513	0.3309	2.7818	25.0	(400)	Cub. Sb_2O_3	1.60	0.0014
	35.0591	0.3310	2.5575	25.2	(331)	Cub. Sb_2O_3	1.58	0.0014
	46.0520	0.4728	1.9693	18.3	(231)	Ortho. Sb_2O_3	3.00	0.0019
	54.5863	0.5201	1.6799	17.2	(113)	Ortho. Sb_2O_3	3.38	0.0020
0.05	27.7554	0.3153	3.2116	26.0	(222)	Cub. Sb_2O_3	1.48	0.0013
	28.4174	0.4729	3.1383	17.3	(121)	Ortho. Sb_2O_3	3.33	0.0020
	46.0404	0.5674	1.9698	15.2	(231)	Ortho. Sb_2O_3	4.32	0.0023
0.1	27.7238	0.3783	3.2152	21.6	(222)	Cub. Sb_2O_3	2.14	0.0016
	28.5120	0.4413	3.1281	18.6	(121)	Ortho. Sb_2O_3	2.90	0.0019
	32.2005	0.4098	2.7777	20.2	(400)	Cub. Sb_2O_3	2.46	0.0017
0.15	27.7238	0.3783	3.2152	21.6	(222)	Cub. Sb_2O_3	2.14	0.0016
	28.4805	0.3783	3.1314	21.7	(121)	Ortho. Sb_2O_3	2.13	0.0016
	30.5296	0.4414	2.9258	18.7	(222)	Cub.In_2O_3	2.87	0.0019
	32.2320	0.5044	2.7750	16.4	(400)	Cub. Sb_2O_3	3.72	0.0021
	35.1324	0.5359	2.5523	15.5	(331)	Cub. Sb_2O_3	4.14	0.0022
	36.5511	0.4099	2.4564	20.4	(200)	Ortho. Sb_2O_3	2.40	0.0017

3-2 Atomic force microscope measurements

The morphologies of Sb_2O_3, Sb_2O_3: WO_3, In_2O_3 nanocomposite thin films were explored with an atomic force microscope (AFM). Figure 3 displays three-dimensional images of the prepared thin films; the obtained data are illustrated in Table 3. The measured values of the average grain size showed a non-regular increase, i.e. decreases and increases, with the increase of the concentration of both oxides in the host material. Table 3 declared that the average grain size decreases by increasing the concentrations of the two oxides up by 0.10 and vice versa. The average roughness also changed by increasing the WO_3 or In_2O_3 concentration. Maximum values of average roughness were 4.343nm and 9.739nm obtained from $(Sb_2O_3)0.95$:$(WO_3)0.05$ and $(Sb_2O_3)0.85$:$(In_2O_3)0.15$ nanocomposite thin films, respectively.

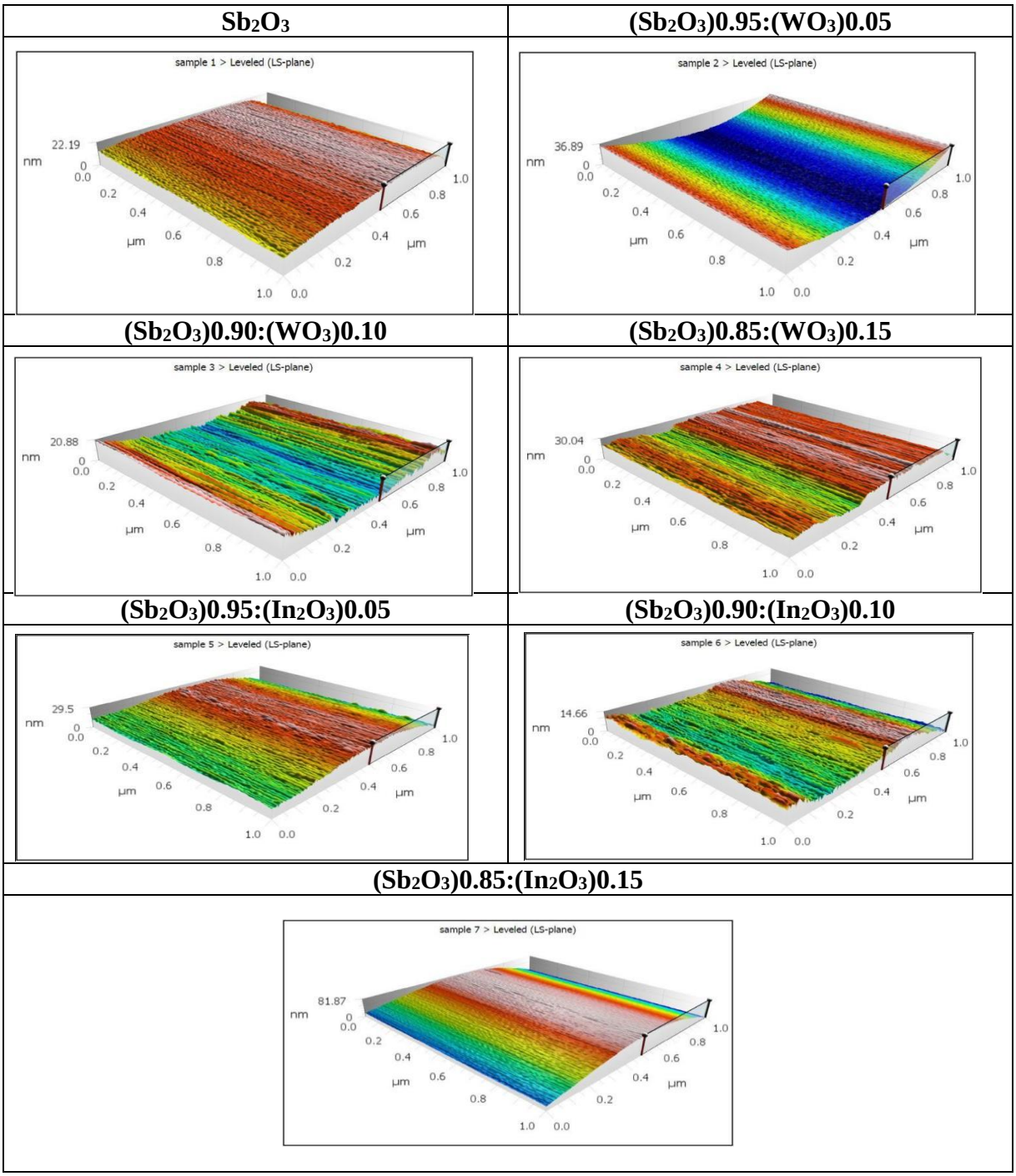

Figure 3: AFM pattern for Sb_2O_3:WO_3, In_2O_3 nanostructure composites thin films

Table 3: The average of the surface roughness and the granular size for the prepared films Sb_2O_3, Sb_2O_3: WO_3, In_2O_3

Sample	Average grain size(nm)	Average roughness(nm)
Sb_2O_3	17.49	1.525
$(Sb_2O_3)0.95:(WO_3)0.05$	14.35	4.343
$(Sb_2O_3)0.95:(WO_3)0.10$	10.10	2.213
$(Sb_2O_3)0.95:(WO_3)0.15$	20.97	3.213
$(Sb_2O_3)0.95:(In_2O_3)0.05$	18.56	2.549
$(Sb_2O_3)0.90:(In_2O_3)0.10$	8.198	1.900
$(Sb_2O_3)0.85:(In_2O_3)0.15$	55.16	9.739

3-3 Optical properties

3-3-1 Optical properties for Sb_2O_3:WO_3 nanocomposite thin films

The optical transmission data were obtained with a UV-Vis spectrophotometer (Shimadzu UV-1800, Made in Japan). The optical properties of Sb_2O_3:WO_3 nanostructures composites thin films were estimated from the transmittance spectra, as shown in Figure 4. It is noticed that the transmittance had shown drastic reduction with the increase of tungsten concentration.

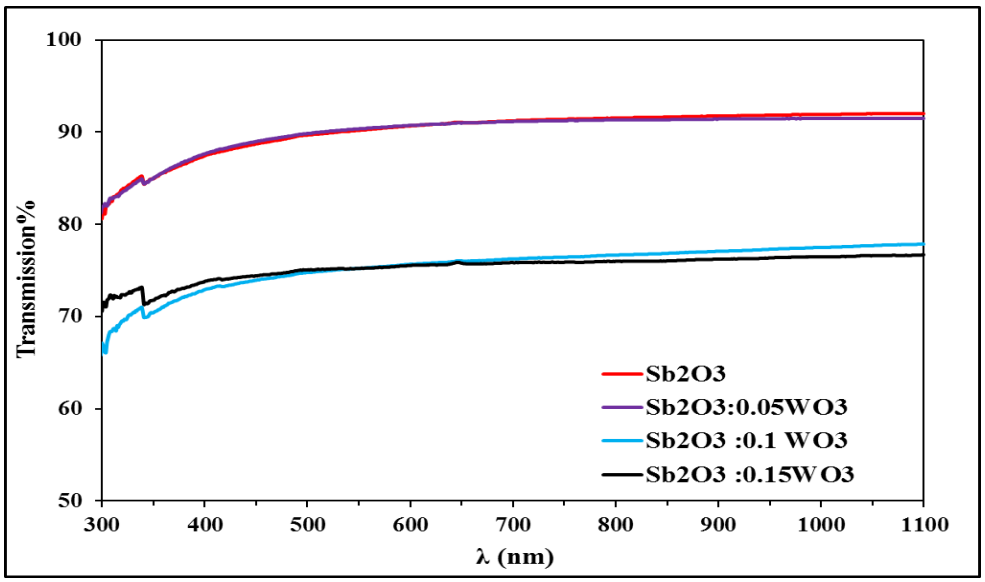

Figure 4: Transmittance spectra of Sb_2O_3:WO_3 nanostructure composite thin films of different WO_3 concentrations.

The band gap energy was estimated using the Tauc equation, as shown in Figure 5. The (r) value was 0.5, indicating a direct allowed transition. The measured values are listed in Table 4. The band gap energy for antimony oxide was 3.3 eV, which agreed with the results of other researchers [21]. The energy gap decreased from 3.3 eV to 2.7 eV by increasing the tungsten oxide concentration. The behavior is attributed to the reduction of transmittance or increase of absorbance. Energy gap energy strongly depends on the crystal structure of the material. Consequently, it depends on the preparative conditions and the preparation process. It is observed experimentally that reduction of the band gap energy occurs when the impurity concentration is particularly high. This effect is called the band gap narrowing effect, ascribed to the emergence of the impurity band formed by the overlap impurity states. Generally, the quantum confinement increases the band gap due to the decrease in the number of orbits participating in the formation of the valance band and the conduction band through orbital overlap. However, the trend doesn't always need to be followed by the material; other parameters can affect the band gap of the material. The predominant phenomena or effect leading to a decrease in the band gap should be figured out, usually the defects. In oxides materials, the quantum size effects show up only below a specific grain size, the reason being that the defect-induced effects are predominant [22]. Band-gap tuning is at the core of current optoelectronic device applications. However, substantial and controllable band-gap tuning is quite challenging in transition metal oxides. In particular, it is possible to tune the band gap by modifying or substituting the metal oxide with another metal oxide. The fascinating physical properties of transition-metal oxides arising from the d-electrons usually disappear with the modified band gap. Such difficulties have hampered the recent searches for more efficient TCO and low band-gap photovoltaic [23].

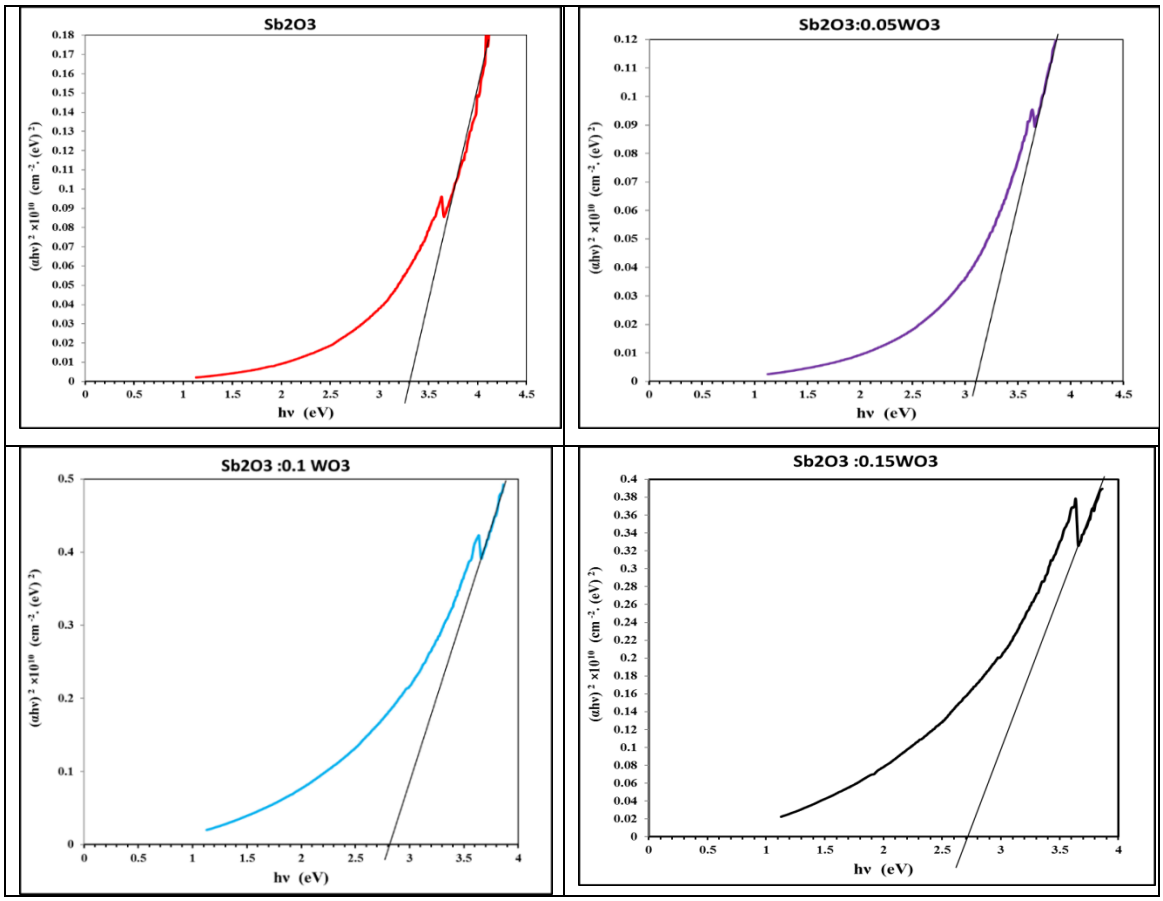

Figure 5: band gap of Sb_2O_3:WO_3 nanostructure composite thin films for the different concentrations of WO_3

Figures (6-9) Illustrate the extinction coefficient, refractive index, real and imaginary parts of the dielectric constant. The addition of WO_3 to antimony oxide will increase the optical constants but the increase was explicit at high WO_3 concentration.

High optical constants have many applications. A refractive index is a measure of how light propagates through a material; the higher the refractive index, the slower the light travels, which causes a correspondingly increased change in the direction of the light within the material. What this means for lenses is that a higher refractive index material can bend the light more and allow the profile of the lens to be lower [24].

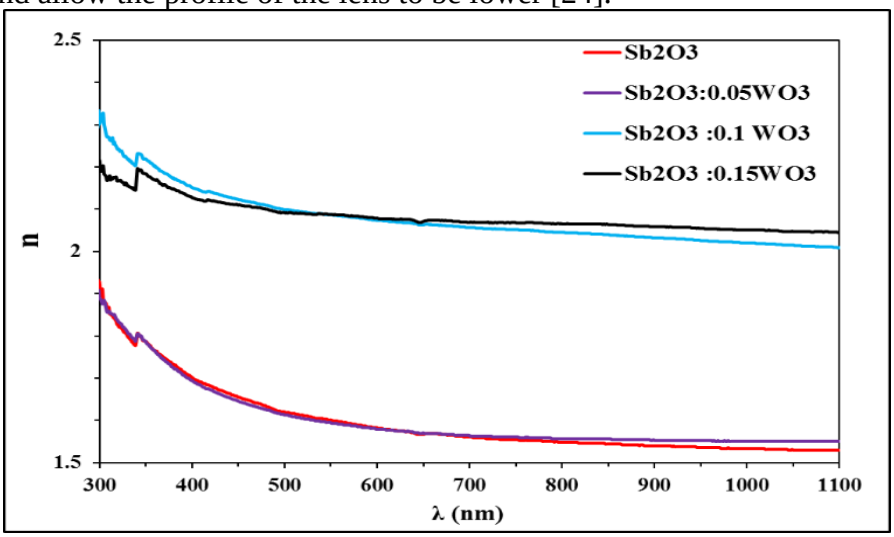

Figure 6: Refractive index as a function of wave-length Sb_2O_3:WO_3 nanostructures composites thin films

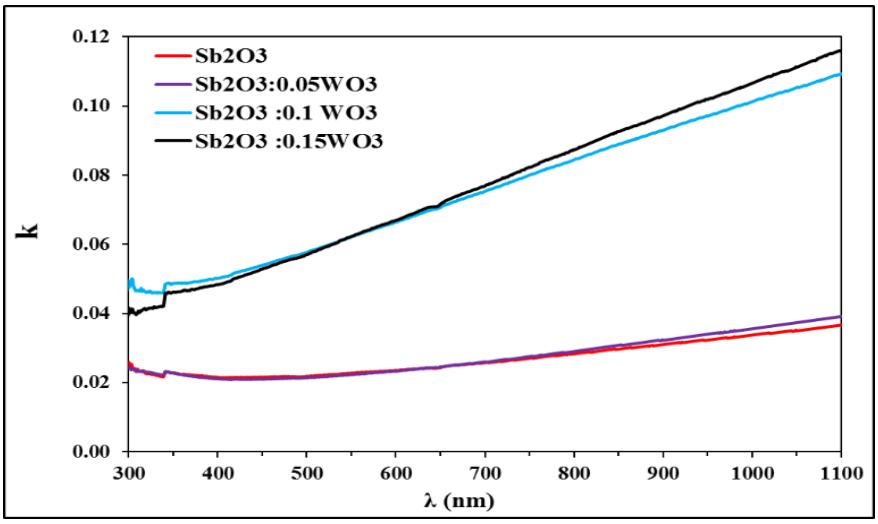

Figure 7: Extinction coefficient as a function of wave-length Sb_2O_3:WO_3 nanostructures composites thin films

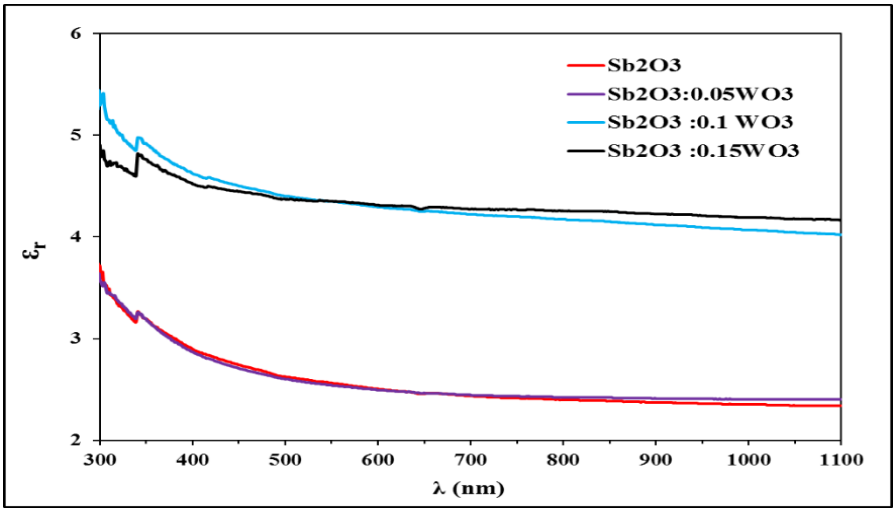

Figure 8: Real dielectric constant as a function of wave-length Sb_2O_3:WO_3 nanostructures composites thin film

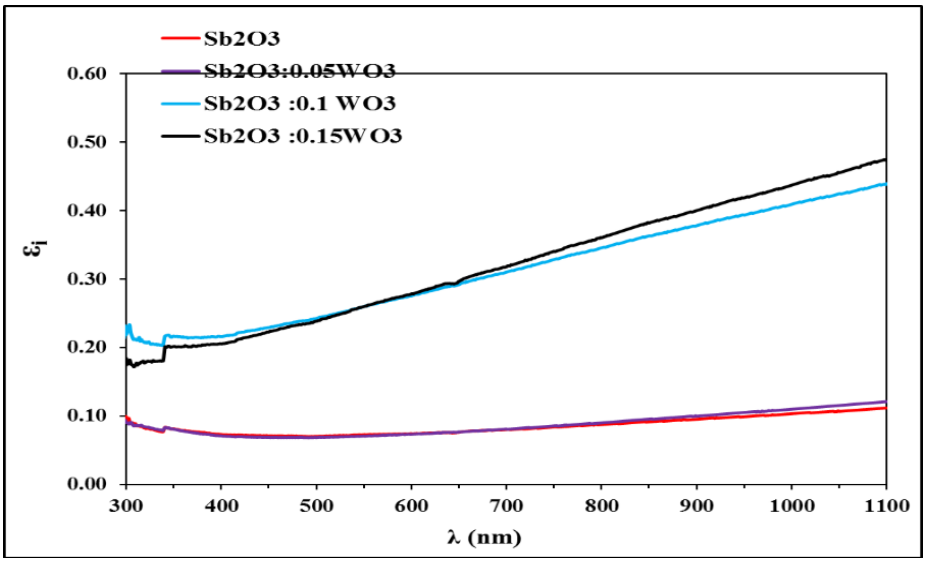

Figure 9: Imaginary dielectric constant as a function of wave-length Sb_2O_3:WO_3 nanostructures composites thin films

Table 4: transmittance, absorption coefficient, optical constants at λ=550nm and optical energy gap Sb_2O_3:WO_3 nanostructures composites thin films

Sample	T%	α (cm^{-1})	k	n	ε_r	ε_i	Eg (eV)
Pure Sb_2O_3	90.16	5182	0.023	1.601	2.564	0.073	3.3
Sb_2O_3:0.05WO_3	90.31	5095	0.022	1.595	2.545	0.071	3.1
Sb_2O_3:0.10WO_3	75.25	14221	0.062	2.087	4.352	0.260	2.8
Sb_2O_3:0.15WO_3	75.25	14221	0.062	2.087	4.352	0.260	2.7

3-3-2 Optical properties for Sb_2O_3:In_2O_3 nanostructures composites thin films

The transmittance spectrum in the wavelength range (300-1100) nm for Sb_2O_3: In_2O_3 nanostructures composites thin film is shown in Figure 10. The transmittance showed a non-regular reduction with the increase in indium oxide concentration. In general, the non-regular decrease of the transmittance by increasing the mixing ratio means an increase in the reflection and absorption, which also means that increasing the mixing ratio makes thin films sample more opaque and less transparent. The shifts of transmittance toward longer wavelength (lower energies) accompanying the increment of mixing ratio are related to the non-regular increase of grain size; the non-regular increase of grain size reduces the lattice parameters and hence reduces the energy gap [25].

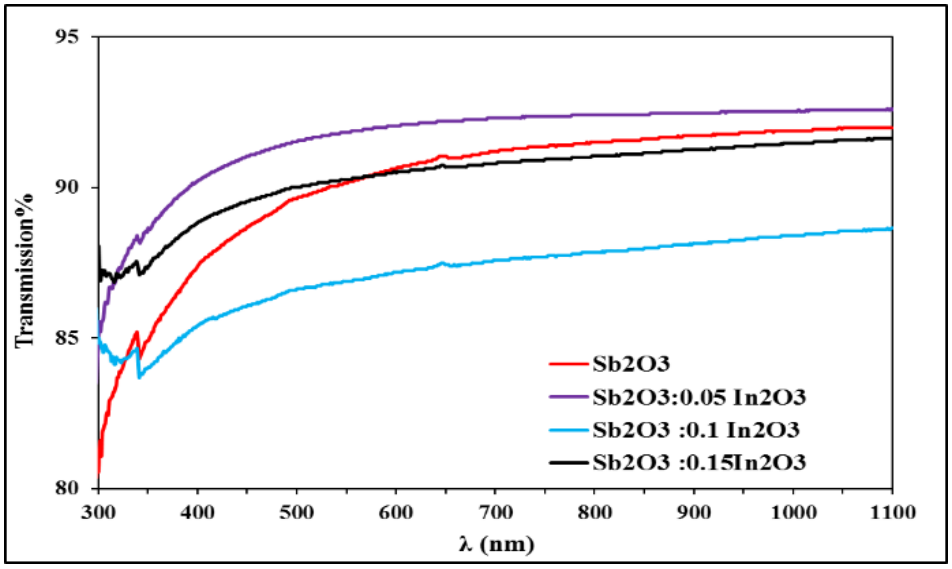

Figure 10: Transmission spectra for Sb_2O_3:In_2O_3 nanostructures composites thin films

The optical energy gap values for direct allowed transition were 3.3, 3.1, 2.9, and 2.8 eV for the different concentrations of antimony oxide and indium oxide.

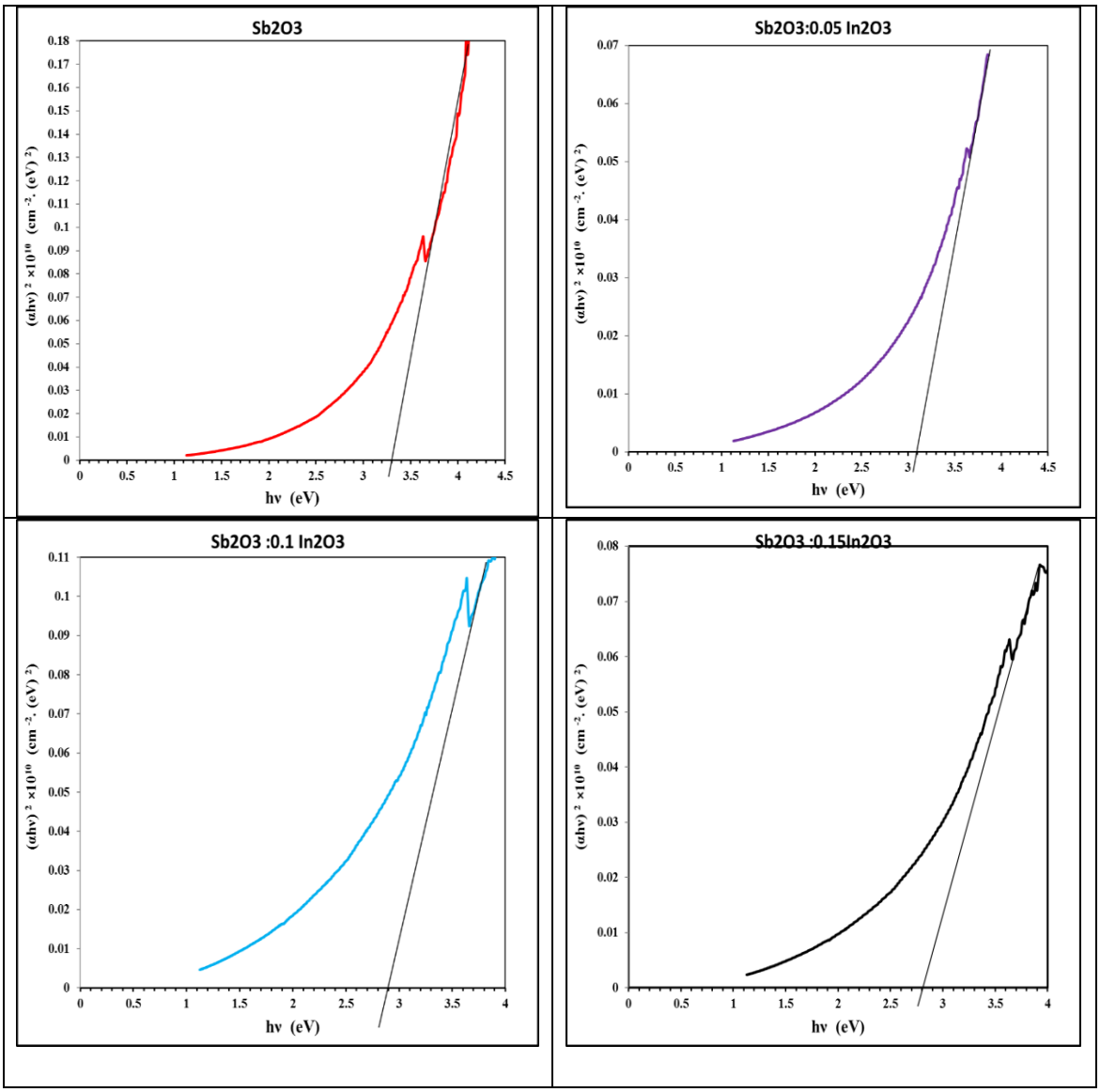

Figure 11: band gap of for Sb_2O_3:In_2O_3 nanostructures composites thin films for different concentration of In_2O_3

Figures (12-15) Illustrate the extinction coefficient, refractive index, real and imaginary parts of the dielectric constant. The addition of In_2O_3 oxide to Sb_2O_3 oxide led to a non-regular reduction of the optical constants. The estimated values of optical constants are listed in Table 5. The behavior explanation of the calculated optical parameters of Sb_2O_3, Sb_2O_3: WO_3, In_2O_3 nanostructures composites thin films can be found elsewhere [26-28]. The optical constants increase by increasing the concentration of indium oxide up 0.1 and then fall with a further increase of indium oxide concentration.

The material selected for the solar cell fabrication should have a high absorption coefficient (α>104cm-1) and a band gap energy within a certain range so that the capturing of light is effective; also, the band gap energy should be in such a range that the incident light ray should excite the electrons present in the material which helps in conversion of the light energy into electrical energy. Therefore, depending on the data obtained and listed in the tables, the best model from which a solar cell can be manufactured is 85%Sb_2O_3:15%WO_3 nanostructures composites thin films, which declared the lowest band gap energy and the highest absorption coefficient.

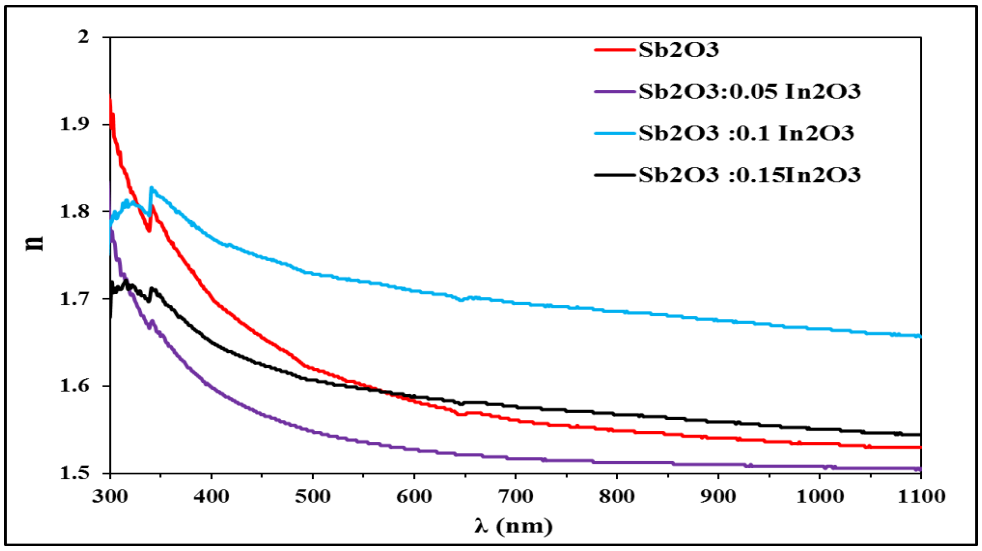

Figure 12: Refractive index as a wave-length function for Sb_2O_3:In_2O_3 nanostructures composites

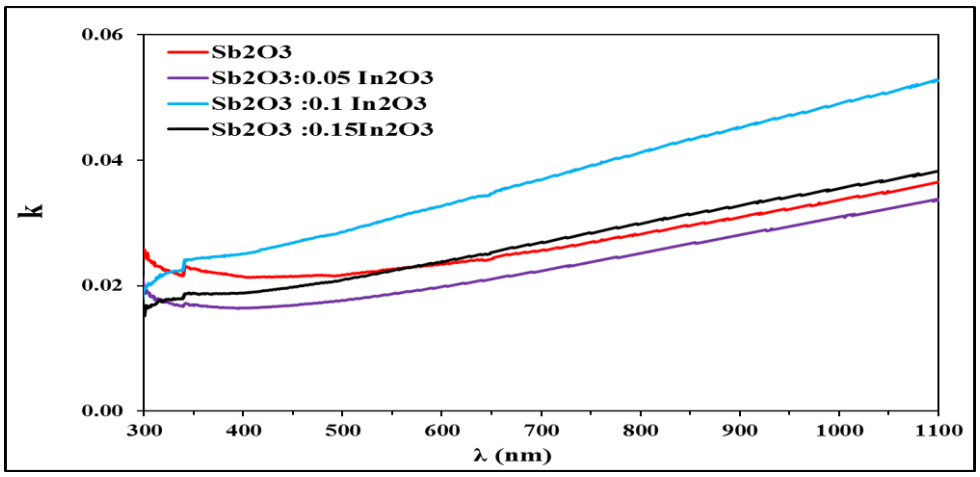

Figure 13: Extinction coefficient as a wave-length function for Sb_2O_3:In_2O_3 nanostructures composites thin films

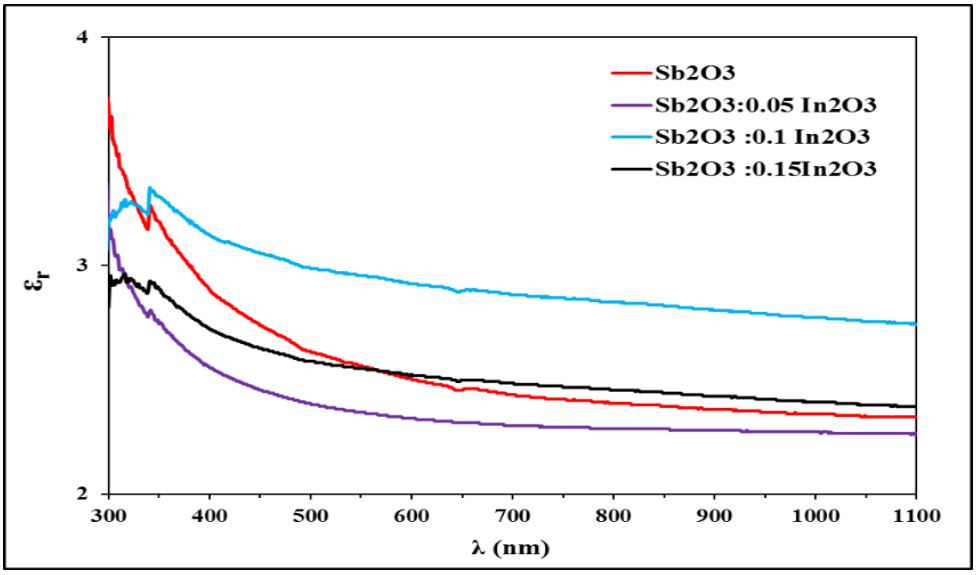

Figure 14: Real dielectric constant as a wave-length function for the Sb_2O_3:In_2O_3 nanostructures composites thin films

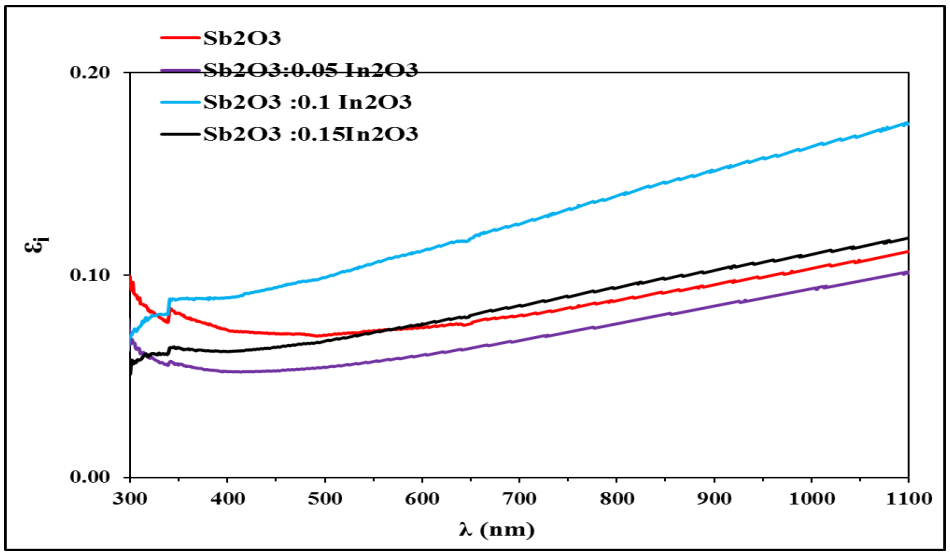

Figure 15: Imaginary dielectric constant as a function of the wavelength for Sb_2O_3:In_2O_3 nanostructures composites thin films

Table 5: The transmittance, absorption coefficient, optical properties, and optical energy gap for Sb_2O_3:In_2O_3 nanostructures composites thin films

Sample	T%	α (cm^{-1})	k	n	ε_r	ε_i	Eg (eV)
Pure Sb_2O_3	90.16	5182	0.023	1.601	2.564	0.073	3.3
Sb_2O_3:0.05In_2O_3	91.83	4261	0.019	1.536	2.359	0.057	3.1
Sb_2O_3:0.10In_2O_3	86.90	7024	0.031	1.720	2.957	0.106	2.9
Sb_2O_3:0.15In_2O_3	90.26	5124	0.022	1.597	2.551	0.072	2.8

4- Conclusions

The dependence of the mixing ratio of (Sb_2O_3: WO_3, In_2O_3) nanocomposite thin films on crystal structure, morphology, and optical properties was investigated. The optical band gap energy decreased with the increasing mixing ratio. This was attributed to the film's high absorption coefficient. Upon increasing the mixing ratio, the structural investigation indicated a reduction in the crystal size of the nanocomposite thin films. The average diameter and roughness were greatly affected by the increase in the mixing ratio. The high roughness value promotes (Sb_2O_3: WO_3,In_2O_3)for gas sensing applications. (Sb_2O_3: WO_3, In_2O_3) nanocomposite thin films showed a directly allowed energy gap, which decreased by increasing the mixing ratio. This was attributed to the film's high absorption coefficient. (Sb_2O_3: WO_3, In_2O_3) nanocomposite thin films showed a high tunable energy gap in the solar spectrum compared to pristine Sb_2O_3 films. This can be ascribed to the WO_3 and In_2O_3 oxides, which act as an electron trap, simplifying charge transport and limiting charge recombination. This makes the (Sb_2O_3: WO_3, In_2O_3) nanocomposite eligible for use in solar cell applications.

References

[1] E., Suroor N. "study the effect of thickness on the optical proprerties of (Sb_2O_3) thin film prepared by thermal evaporation technique." *Journal of College of Education*, the first issue 2, 2012.

[2] M. R. Mahmood, M. A. Habeeb, and A. Hashim, "Effect of antimony oxide nanoparticles on structural, optical and AC electrical properties of (PEO-PVA) blend for antibacterial applications," *Int. J.*, vol. 8, no. 8, pp. 4726 – 4738, 2020.

[3] H. S. Hakeen and N. K. Abbas, "Preparing and studying structural and optical properties of Pb1-xCdxS nanoparticles of solar cells applications," *Baghdad Science Journal*, vol. 18, no. 3, pp. 0640-0640, 2021.

[4] F. Z. Agti, M. T. Soltani, L. F. Santos, A. Messaoudi, N. Guesmia, and D. D. Ligny,"Physical, mechanical properties and optical dispersion in Sb_2O_3-NaPO3-WO_3 glasses," *Journal of Non-Crystalline Solids*, vol. 576, no. 2, pp. 121249, 2022.

[5] K. V. Divya, and K. E. Abraham, "Ag nanoparticle decorated Sb2O3 thin film: synthesis, characterizations and application," *Nano Express*, vol. 1, no. 2, p. 020005, 2020.

[6] Y. Peng, J. Chen, L. Jiang, T. Wang, H. Yang, F. Liu, M. Jia,"Preparation of Sb_2O_3/Sb_2S_3/FeOOH composite photoanodes for enhanced photoelectrochemical water oxidation," *Transactions of Nonferrous Metals Society of China*, vol. 30, no. 6, pp. 1625-1634, 2020.

[7] L. Jian, C. Hong, Yan and Z. Libo, "Basic study on microwave carbon-thermal reduction senarmontite (Sb_2O_3) to produce antimony: High-temperature dielectric properties and a microwave reduction mechanism," *Powder Technology*, vol. 389, pp. 482-492, 2021.

[8] Y. P. Shinde, "Engineering of physical properties of spray-deposited nanocrystalline Sb_2O_3 thin films by phase transformation," *Nanotechnology*, vol. 32, no. 2, p. 025602, 2020.

[9] W. Qi, S. Guo, H. Sun, Q. Liu, H. Hu, P. Liu, W. Lin, M. Zhang, "Synthesis and characterization of Sb_2O_3 nanoparticles by liquid phase method under acidic condition," *Journal of Crystal Growth*, vol. 588, pp. 126642, 2022.

[10] H. H. Abbas and B. A. Hasan "The Effect of Silver Oxide on the Structural and Optical Properties of ZnO: AgO Thin Films," *Iraqi Journal of Science*, vol. 63, no. 4, pp. 1526-1539, 2022.

[11] J. Epp, "X-Ray Diffraction (XRD) Techniques for Materials Characterization." *Elsevier Ltd*, 2016.

[12] Kazmerski, Lawrence, "Polycrystalline and amorphous thin films and devices." *Elsevier*, 2012.

[13] Piprek, Joachim. "Semiconductor optoelectronic devices: introduction to physics and simulation." *Elsevier*, 2013.

[14] Y. C. Liang, C. W. Chang, "Preparation of orthorhombic WO3 thin films and their crystal quality-dependent dye photodegradation ability," *Coatings*., vol. 9, no. 2, pp. 90, 2019.

[15] R. Shakoury, A. Arman, S. Rezaee, A. G. Korpi, S. Kulesza, C. Luna, M. Bramowicz, M. Mardani, "Optical properties and morphology analysis of hexagonal WO_3 thin films obtained by electron beam evaporation." *Journal of Materials Science: Materials in Electronics*, vol. 32, pp. 798-805, 2021.

[16] S. K. Neogi, S. Chattopadhyay, A. Banerjee, S. Bandyopadhyay, A. Sarkar, R. Kumar, "Effect of 50 MeV Li3+irradiation onstructural and electrical properties of Mn doped ZnO," *J. Phys. Condens. Matter*., vol. 23, p. 205801, 2011.

[17] S. I. Salih, "Effect of Sb_2O_3 and/or CdO nanoparticle substitution on the properties of high-TC superconducting Bi1.6-x SbxPb0.4Sr2Ca2-yCdyCu3OZ material," *IJP*, vol. 16, no. 36, pp. 73–84, 2018.

[18] A. Yahia, A. Attaf, H. Saidi, M. Dahnoun, C. Khelifi, A. Bouhdjer, & H. Ezzaouia,"Structural, optical, morphological and electrical properties of indium oxide thin films prepared by sol gel spin coating process," *Surfaces and Interfaces*, vol. 14, pp. 158-165, 2019.

[19] Lin, H., Wei, Q., Ke, B., Lin, W., Zhao, H., & Zou, B. "Excitation-Wavelength-Dependent Emission Behavior in (NH4) 2SnCl6 via Sb3+ Dopant." *The Journal of Physical Chemistry Letters*, vol. 14, no. 6, pp. 1460-1469, 2023.

[20] Mahdi, A. Aws, and S. A. Makki, "Study the Effect of Annealing on the Structural Properties of Zinc Oxide Films by Electrolysis Technique," *Ibn AL-Haitham Journal For Pure and Applied Sciences*, vol. 34, no. 1, pp. 12-18, 2021.

[21] Sun, G., Li, B., Wang, S., Zhang, Z., Li, J., & X. Duan,"Selective growth of wide band gap atomically thin Sb 2 O 3 inorganic molecular crystal on WS 2," *Nano Research*, vol. 12, pp. 2781-2787, 2019.

[22] M. M. Hameed, A. E. Al-Samarai, and K. A. Aadim, "Synthesis and characterization of gallium oxide nanoparticles using pulsed laser deposition." *Iraqi Journal of Science*, vol. 61, no. 10, pp. 2582-2589, 2020.

[23] Hyun Jin Julie Yua , Patrice Geoffron ,"Photovoltaic Solar Energy Conversion Technologies, Applications and Environmental Impacts," *Academic Press*, pp. 413-437, 2020.

[24] A. Khalid Haneen, and N. H. Obaid, "0.006 wt.% Ag-Doped Sb_2O_3 Nanofilms with Various Thickness: Morphological and optical properties," *Journal of Physics: Conference Series*, vol. 1294, no. 2. IOP Publishing, 2019.

[25] B. A. Hasan and R. M. Abdallah, "The role of tin oxide concentration on the x-ray diffraction, morphology and optical properties of In_2O_3: SnO_2 thin films," *Journal of Physics: Conference Series*, vol. 1003, no. 1, IOP Publishing, 2018.

[26] B. A. Hasan, S. S. Mahmood, H. H.Issa,T. T. Issa,"Structural, Morphology and Optical Properties

[27] ofAlxSb1-x Thin Films Prepared by Pulsed Laser Deposition(PLD)," *AIP Conference Proceedings*

[28] vol. 2372, p. 040010, 2021.

[29] W. A. Al-Taa'y, and B. A. Hasan, "Structural and optical properties of TiO2: NiO nanoparticles thin films prepare by chemical spray pyrolysis," *Iraqi Journal of Physics*, vol. 19, no. 49, pp. 22-31, 2021.

[30] M. A. Abood, and B. A. Hasan, "A Comparison Study the Effect of Doping by Ga2O3 and CeO2 On the Structural and Optical Properties of SnO_2 Thin Films," *Iraqi Journal of Science*, vol. 64, no. 4, pp. 1675-1690, 2023.